Model predictive control with finite constant set for five-level neutral-point clamped inverter fed interior permanent magnet synchronous motor drive of electric vehicle

Tran Hung Cuong[1], An Thi Hoai Thu Anh[2]
[1]Faculty of Electrical and Electronic Engineering, Thuyloi University, Hanoi, Vietnam
[2]Faculty of Electrical and Electronics Engineering, University of Transport and Communications, Hanoi, Vietnam

Article Info

Article history:

Received Apr 17, 2024
Revised Jul 11, 2024
Accepted Jul 17, 2024

Keywords:

Balancing voltage capacitor
Controller for electric cars
Energy saving
Finite control set-model predictive control
Neutral-point clamped inverter

ABSTRACT

This paper uses the five-level neutral-point clamped (NPC) inverter to feed an electric vehicle's traction motor-interior permanent magnet synchronous motor (IPMSM). The model predictive control method controls the energy conversion process according to the model with two prediction steps. The advantage of this method is its fast response, which increases the ability to operate the converter with good voltage quality. Model predictive control (MPC) control is a closed-loop strategy with much potential when integrating multiple control objectives; the calculation process is compact without complex modulation. Within the scope of this article, the MPC strategy will be implemented with two control goals for NPC, including output load current and capacitor voltage balance with low switching frequency. The simulation results on MATLAB/Simulink software were performed to verify the proposed algorithm's effectiveness in minimizing the grid current's harmonics and ensuring an uninterrupted power supply.

Corresponding Author:

An Thi Hoai Thu Anh
Department of Electrical Engineering, Faculty of Electrical-Electronic Engineering, University of Transport and Communications
No 3 Cau Giay, Lang Thuong Commune, Dong Da District, Hanoi, Vietnam
Email: htanh.ktd@utc.edu.vn

1. INTRODUCTION

Recently, power electronic converters have played an essential role in improving the quality of output voltage supplied to traction motors of electric vehicles. Several inverter topologies that can be used have been reported in [1]–[3]; one of the most promising inverters is the NPC multilevel inverter (point clamped neutral inverter). Neutral-point clamped (NPC) is widely used in alternating current (AC) drive applications and power electronics systems. Because it can provide a variety of output AC voltage levels. Therefore, NPC is suitable for voltage levels from low, medium, and high [4], [5]. This significantly reduces the voltage stress on the semiconductor valves during operation. With this inverter, it is possible to increase the value of conversion capacity and simplify the process of selecting filter parameters to improve filtering ability more effectively. The harmonic quality of current and voltage is improved [6]. The disadvantage of this configuration is that it is necessary to balance the direct current (DC) link capacitor voltage value when implementing control measures [4]. Controlling the NPC inverter is important because it determines the quality of operation and overall performance of the system. Many control techniques have been reported in the literature [7]–[11]; Most of them are focused on improving the quality of current and voltage and balancing the voltage on capacitors. Modulation methods for NPC are also introduced in [12]–[14] including space vector modulation (SVM) and pulse width modulation (PWM) modulation algorithms. However, the combination of control and modulation algorithms still has many disadvantages, such as slow response and the effectiveness of DC-link capacitor voltage balance not being stable. Recently, model predictive control (MPC) has been researched and applied in power electronics because it has many advantages, such as fast, accurate and stable action. The documents present research for MPC control in power electronics [15]–[21]. The goal is to exploit NPC performance. This paper studies the finite control set-model predictive control (FCS-MPC) method to apply to NPC inverter. The goal is to control many parameters simultaneously, such as output load current and capacitor voltage balance. This method uses discrete-time models of the converter and load to predict the future behaviour of the load current and DC-link capacitor voltage for all possible switching states. This study uses a two-step prediction model to improve load current regulation to improve converter performance to create the quality of voltage to feed interior permanent magnet synchronous motor (IPMSM).

2. MODEL OF NPC INVERTER FED IPMSM

An electric car's drive system comprises the interior permanent magnet (IPM) motor fed by an NPC inverter. This drive system's modelling includes the IPM motor and the forces acting on it is using the field-oriented control (FOC) method and a 5-level NPC inverter with predictive control. In this system, the motor provides the traction force for the car to move, and the NPC inverter provides energy for the car's traction motor to operate.

2.1. Modeling the IPM motor and external forces

The IPM motor with the FOC control method is built upon the dq coordinate system due to its modelling and control design advantages. With inductances L_d different from L_q, the motor torque includes an additional component and the reluctance torque. The mathematical equations describe the motor as (1):

$$\begin{cases} \frac{di_{sd}}{dt} = -\frac{1}{T_{sd}} i_{sd} + \omega_s \frac{L_{sq}}{L_{sd}} i_{sq} + \frac{1}{L_{sd}} U_{sd} \\ \frac{di_{sq}}{dt} = -\omega_s \frac{L_{sq}}{L_{sd}} i_{sd} - \frac{1}{T_{sq}} i_{sq} + \frac{1}{L_{sq}} U_{sq} - \omega_s \frac{\psi_p}{L_{sq}} \\ \psi_{sd} = L_{sd} i_{sd} + \psi_p \\ \psi_{sq} = L_{sq} i_{sq} \\ T_e = \frac{3}{2} p_p (\psi_p i_{sq} - i_{sd} i_{sq} (L_{sd} - L_{sq})) \\ T_e - T_L = \frac{J}{p_p} \frac{d\omega}{dt} \end{cases} \quad (1)$$

where U_{sd}, U_{sq}, i_{sd} , i_{sq}, ψ_{sd}, ψ_{sq} are voltages, currents, and fluxes of the stator on d and q-axis; R_s, L_{sd}, and L_{sq} are the stator resistance, the stator inductances on dq, ω_s is the angular velocity of the motor, ψ_p is the rotor flux, p_p is the number of pole pairs of the motor; T_e, T_L are the motor output torque, the load torque; J is the moment of inertia of the motor, $T_{sd} = \frac{L_{sd}}{R_s}$ is the d-axis time constant of the stator circuit and is the q-axis time constant of the stator.

As the vehicle moves, resistance forces comprise of two components: air resistance and the vehicle's friction with the air [22]–[24]. These two components combined form the wind resistance force as (2):

$$F_{wind} = \frac{1}{2} \rho C_d A_f (v_{veh} + v_{wind})^2 \quad (2)$$

Where ρ is the air density, C_d is the coefficient of air resistance (typically: $0.2 < C_d < 0.4$) and A_f is the frontal area of the vehicle's body (cross-sectional area), and v_{wind} is the wind speed. The rolling friction force can be calculated as [25]:

$$F_{roll} = f_r m_v g \cos \alpha \quad (3)$$

where m_v is the total mass of the vehicle and passengers, g is the gravitational acceleration, α is the slope angle, f_r is the coefficient of rolling resistance calculated by the formula:

$$f_r = 0.01 \left(1 + \frac{3.6}{100} v_{veh}\right) \quad (4)$$

With v_{veh} being the velocity of the vehicle.

2.2. Modeling the NPC inverter

The NPC converter in this study is a three-phase inverter, which structure includes four legs and five voltage levels, the output filter of which is shown in Figure 1. This structure differs from the basic NPC inverter which is additional an additional leg connected to the neutral point of the load. The inverter includes 16 semiconductor valves and 8 clamping diodes. Table 1 describes the switching states corresponding to the inverter terminal voltage.

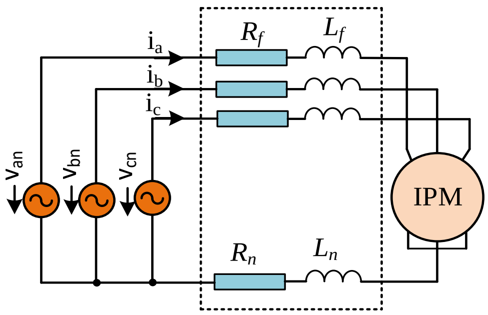

Figure 1. Schematic of NPC structure replacement connected to IPM

Table 1. The output voltage of the NPC inverter corresponds to the IGBT valve switching states (x = a, b, c, n)

S_x	S_{1x}	S_{2x}	S_{3x}	S_{4x}	v_{xN}
1	1	1	0	0	$v_{c1} + v_{c2}$
0	0	1	1	0	v_{c2}
-1	0	0	1	1	0

According to Table 1, the number of available switching combinations for this variable can be calculated as 81(3^4). The voltage in each phase of the inverter is measured from the negative point of the DC-link (N) and the middle point of each phase and is expressed in terms of the valve switching state and the voltage of the DC capacitors as (5):

$$\begin{bmatrix} v_{an} \\ v_{bn} \\ v_{cn} \\ v_{nN} \end{bmatrix} = v_{c1} \begin{bmatrix} S_{1a} \\ S_{1b} \\ S_{1c} \\ S_{1n} \end{bmatrix} + v_{c2} \begin{bmatrix} S_{2a} \\ S_{2b} \\ S_{2c} \\ S_{2n} \end{bmatrix} \tag{5}$$

The inverter's output voltages are expressed as the midpoint (n) of the neutral point as (6).

$$\begin{bmatrix} v_{an} \\ v_{bn} \\ v_{cn} \end{bmatrix} = \begin{bmatrix} v_{aN} - v_{nN} \\ v_{bN} - v_{nN} \\ v_{cN} - v_{nN} \end{bmatrix} \tag{6}$$

Solving (1) and (2) yields the load voltage, which is written as (7).

$$\begin{bmatrix} v_{an} \\ v_{bn} \\ v_{cn} \end{bmatrix} = v_{c1} \begin{bmatrix} S_{1a} - S_{1n} \\ S_{1b} - S_{1n} \\ S_{1c} - S_{1n} \end{bmatrix} + v_{c2} \begin{bmatrix} S_{2a} - S_{2n} \\ S_{2b} - S_{2n} \\ S_{2c} - S_{2n} \end{bmatrix} \tag{7}$$

From (7), it can be considered that each branch in a phase of the NPC is equivalent to a voltage source. Therefore, the equivalent diagram of the inverter is shown in Figure 1, where n and o are the converter neutral and the load, respectively. According to Kirchhoff's law applies to the current and voltage in the circuit of Figure 1, the AC side voltage of the inverter is expressed as (8):

$$\begin{bmatrix} v_{an} \\ v_{bn} \\ v_{cn} \end{bmatrix} = R_f \begin{bmatrix} i_a \\ i_b \\ i_c \end{bmatrix} + L_f \frac{d}{dt} \begin{bmatrix} i_a \\ i_b \\ i_c \end{bmatrix} + \begin{bmatrix} R_a & 0 & 0 \\ 0 & R_b & 0 \\ 0 & 0 & R_c \end{bmatrix} \begin{bmatrix} i_a \\ i_b \\ i_c \end{bmatrix} - R_n i_n - L_n \frac{d}{dt} i_n \tag{8}$$

where $R_f = R_{fa} = R_{fb} = R_{fc}$ *và* $L_f = L_{fa} = L_{fb} = L_{fc}$

In Figure 1, we can determine the equation that describes the relationship between the neutral load current and the load current as (9).

$$i_n = -(i_a + i_b + i_c) \tag{9}$$

By substituting (9) into (8), the AC side voltage of the inverter can be expressed independently of the neutral current of the load as (10).

$$\begin{bmatrix} v_{an} \\ v_{bn} \\ v_{cn} \end{bmatrix} = R_{eq} \begin{bmatrix} i_a \\ i_b \\ i_c \end{bmatrix} + L_{eq} \frac{d}{dt} \begin{bmatrix} i_a \\ i_b \\ i_c \end{bmatrix} \tag{10}$$

In there: $R_{eq} = \begin{bmatrix} R_f + R_n + R_a & 0 & 0 \\ 0 & R_f + R_n + R_a & 0 \\ 0 & 0 & R_f + R_n + R_a \end{bmatrix}$; $L_{eq} = \begin{bmatrix} L_f + L_n & L_n & L_n \\ L_n & L_f + L_n & L_n \\ L_n & L_n & L_f + L_n \end{bmatrix}$

Performing differential (10), we get the differential equation of load current as (11).

$$\frac{d}{dt} \begin{bmatrix} i_a \\ i_b \\ i_c \end{bmatrix} = L_{eq}^{-1} R_{eq} \begin{bmatrix} i_a \\ i_b \\ i_c \end{bmatrix} + L_{eq}^{-1} \begin{bmatrix} v_{an} \\ v_{bn} \\ v_{cn} \end{bmatrix} \tag{11}$$

Relationship between the DC-link capacitor voltage through the DC-link capacitor current presented as (12).

$$\begin{cases} \frac{d}{dt} v_{c1} = \frac{1}{C_1} i_{dc1} \\ \frac{d}{dt} v_{c2} = \frac{1}{C_2} i_{dc2} \end{cases} \tag{12}$$

where the currents i_{dc1} and i_{dc2} are calculated according to the three-phase load currents (i_a, i_b and i_c) and the switching states of the inverter are as (13):

$$\begin{cases} i_{dc1} = K_a . i_a + K_b . i_b + K_c . i_c \\ i_{dc2} = Q_a . i_a + Q_b . i_b + Q_c . i_c \end{cases} \tag{13}$$

Here K_x and Q_x represent the level voltage, expressly:

$$\begin{aligned} K_x &= sgn\{S_n - 1\} - sgn\{S_x - 1\} \\ Q_x &= sgn\{S_n + 1\} - sgn\{S_x + 1\} \end{aligned} \tag{14}$$

where S_n and S_x are the switching states correspond to neutral levels and phase. sgn is an argument sign whose value corresponds to 0, 1, or −1. From on (7) and (9), We can determine the switching states related to the value of the load current and voltage of the DC-link capacitor. Furthermore, they are controlled by selecting appropriate switching states.

3. FINITE CONTROL SET - MODEL PREDICTIVE CONTROL FOR NPC

3.1. Control strategy

Figure 2 shows the FCS-MPC control proposed for NPC to adjust the load current and balance the voltage of the DC-link capacitor. This method uses a discrete system model, the current states (time k). The advantage of this method is that it does not need to use a PI controller and modulation stage like other methods, so it reduces complexity in model implementation. When continuing the prediction in step 2 (N=2), the number of switching states will increase. This process will require more computation by the controller. However, it will perform better than a one-step prediction and reduce the valve switching frequency [18]. To minimize the calculation of the inverter's switching steps at time k+2, in this article, the algorithm will select the best state at prediction step k and eliminate unnecessary states to perform k+2 prediction steps, and the best working state that minimizes the objective function will be selected, the process is shown in Figure 3. The next process is repeated throughout the inverter's working time.

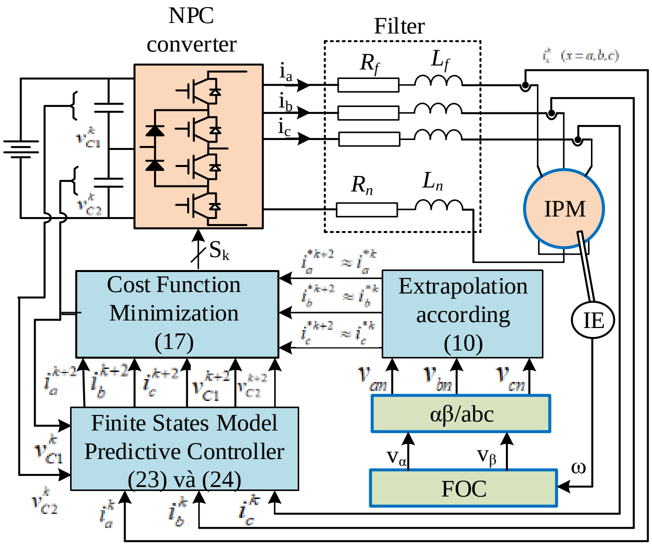

Figure 2. FCS-MPC control structure for NPC inverter combined with FOC control algorithm

3.2. Build up the cost function

The cost function is determined to have two goals: minimize the error between the predicted load current i^{k+2} and its set value at time $k+2$ (i^{*k+2}); and the voltage balance of DC-link capacitors. These two goals are expressed as (15).

$$J_{ix}^{k+2} = [i_x^{*k+2} - i_x^{k+2}]^2; J_{vc}^{k+2} = \lambda_{dc}[v_{c1}^{k+2} - v_{c2}^{k+2}]^2 (x = a, b, c) \tag{15}$$

where λ_{dc} is the weighting coefficient, its value is adjusted according to the desired performance.

However, because the set value during NPC operation is constant, it can be considered that the set value at time k+2 is approximately equal to the set value at time k. Then the cost function (15) is rewritten as (16).

$$J_{ix}^{k+2} = [i_x^{*k+2} - i_x^{k}]^2; J_{vc}^{k+2} = \lambda_{dc}[v_{c1}^{k+2} - v_{c2}^{k+2}]^2 \tag{16}$$

From (16), it can be deduced that the overall cost function for the control objective is as (17):

$$J^{k+2} = J_{ix}^{k+2} + J_{vc}^{k+2} \tag{17}$$

The transition state to minimize the cost function is selected and used to apply at the next sampling time in a continuously repeating cycle.

3.3. Mathematical relationship with two-step prediction of variables

As analyzed in Figure 3(a), the objective function must give the predicted load current value i^k+2 and capacitor voltage $v_{c1}^{k+2}$and v_{c2}^{k+2} in discrete time form. To do this, the predicted load current is obtained from the continuous-time state model of the system from formula (11) and is expressed:

$$\begin{bmatrix} i_a^{k+1} \\ i_b^{k+1} \\ i_c^{k+1} \end{bmatrix} = P \begin{bmatrix} i_a^{k} \\ i_b^{k} \\ i_c^{k} \end{bmatrix} + Q \begin{bmatrix} v_{an}^{k} \\ v_{bn}^{k} \\ v_{cn}^{k} \end{bmatrix} \tag{18}$$

In there: $P = e^{-L_{eq}^{-1}R_{eq}T_s}$; $H = \int_0^{T_s} e^{-L_{eq}^{-1}R_{eq}T_s} L_{eq}^{-1} dt = \left(-L_{eq}^{-1}R_{eq}\right)^{-1}(P - I_{3x3})L_{eq}^{-1}$, continue with the interruption of the predicted load current at time k+2 described:

$$\begin{bmatrix} i_a^{k+2} \\ i_b^{k+2} \\ i_c^{k+2} \end{bmatrix} = P \begin{bmatrix} i_a^{k+1} \\ i_b^{k+1} \\ i_c^{k+1} \end{bmatrix} + H \begin{bmatrix} v_{an}^{k} \\ v_{bn}^{k} \\ v_{cn}^{k} \end{bmatrix} \tag{19}$$

This equation demonstrates the first-order dynamics of the model describing the system in (5)-(14). Therefore, this paper only considers the first-order Euler approximation for the derivative with enough accuracy as (20):

$$\frac{d}{dt}x = \frac{1}{T_S}(x^{k+1} - x^k) \tag{20}$$

By substituting (16) in (8), the voltage of the DC-link capacitor is expressed as a discrete-time as (21):

$$\begin{cases} v_{c1}^{k+1} = v_{c1}^{k} + \frac{T_s}{C_1} i_{dc1}^{k+1} \\ v_{c2}^{k+1} = v_{c2}^{k} + \frac{T_s}{C_2} i_{dc2}^{k+1} \end{cases} \tag{21}$$

where T_s is the sampling time, C_1 and C_2 are the capacitance of the two DC-link capacitors respectively. The DC-link capacitor current is expressed in discrete time as (22).

$$\begin{cases} i_{dc1}^{k+1} = K_a.i_a^k + K_b.i_b^k + K_c.i_c^k \\ i_{dc2}^{k+1} = Q_a.i_a^k + Q_b.i_b^k + Q_c.i_c^k \end{cases} \tag{22}$$

By converting the variables into a future sample, we get the voltage of the DC-link capacitor for two-step prediction is obtained as shown in (23).

$$\begin{cases} v_{c1}^{k+2} = v_{c1}^{k+1} + \frac{T_s}{C_1} i_{dc1}^{k+2} \\ v_{c2}^{k+2} = v_{c2}^{k+1} + \frac{T_s}{C_2} i_{dc2}^{k+2} \end{cases} \tag{23}$$

In there:

$$\begin{cases} i_{dc1}^{k+2} = K_a.i_a^{k+1} + K_b.i_b^{k+1} + K_c.i_c^{k+1} \\ i_{dc2}^{k+2} = Q_a.i_a^{k+1} + Q_b.i_b^{k+1} + Q_c.i_c^{k+1} \end{cases} \tag{24}$$

From the above analysis and construction of the control model, the flow chart describes the algorithm as shown in Figure 3(b).

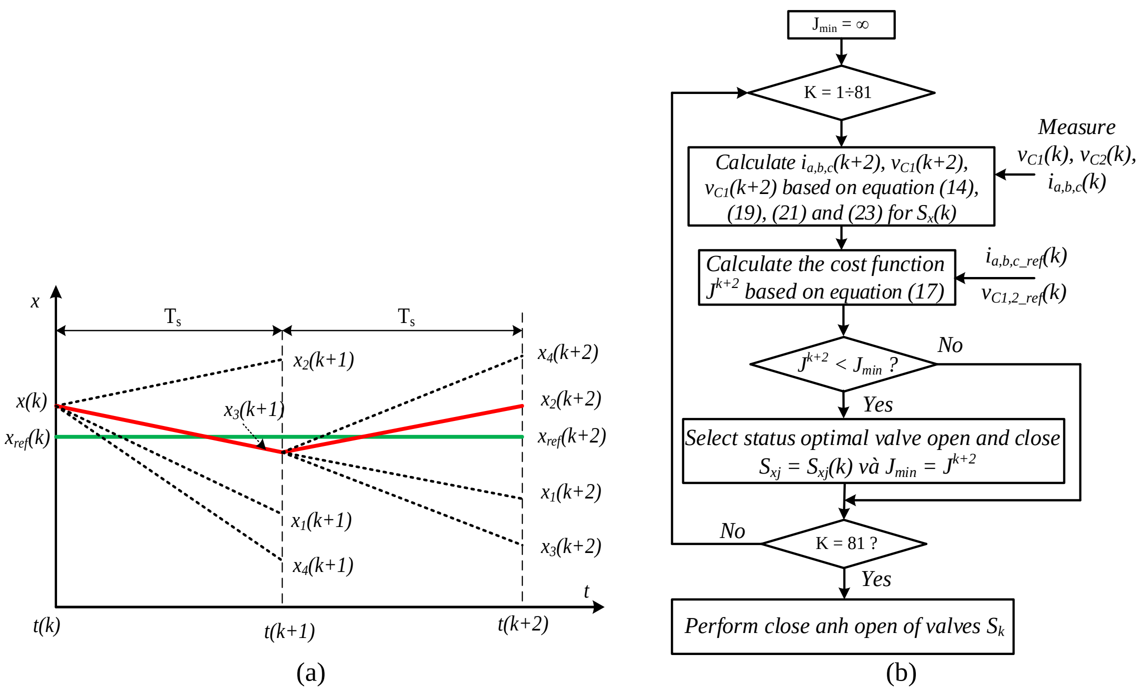

Figure 3. Predictive control principles (a) description of the two-step signal prediction state of the FCS-MPC control strategy and (b) algorithm flow chart of FCS-MPC control strategy for NPC

4. SIMULATION RESULTS OF FCS-MPC CONTROL STRATEGY FOR NPC

In section 4, the speed, current, and voltage responses will be evaluated when applying the predictive control strategy for the 5-level NPC inverter model and FOC control design for the IPM motor drive for electric vehicles. The simulation parameters of the electric vehicle are indicated in Tables 2 and 3. The testing conditions are based on the standard urban cycle of Europe ECE [26].

Table 2. Parameters of IPM motor

Parameters	Symbol	Value	Unit
Stator resistance	R_s	6.5e-3	Ohm
d-axis inductance	L_{sd}	1.597e-3	H
q-axis inductance	L_{sq}	2.057e-3	H
Moment of inertia	J	0.09	kg.m^2
Number of pole pairs	p_p	4	
DC voltage	V_{dc}	550	V

Table 3. Parameters of electric car and the environment

Parameters	Value	Unit
Vehicle weight + load	2018	kg
Wheel radius	0.3	m
Transmission ratio	9.73	
Maximum speed	130	km/h
Effective area	2.3	m^2
Air density	1.25	kg/m^3
Road gradient	0	
Rolling resistance coefficient	0.02	

Figures 4 to 6 demonstrate the system's responses. Figure 4 shows the response of the reference speed curve based on the standard urban cycle of Europe ECE coincident with that of the actual speed curve with three modes of operation: accelerating, holding, and braking. Figure 5 demonstrates that the output voltage has a five-level form and no transients; the levels are always stable in all three phases. The voltage on capacitors C_1 and C_2 is shown in Figure 6, and the voltages of capacitors v_{c1} and v_{c2} always stick to their rated value of 275 V, corresponding to half the voltage. DC-bus V_{DC}, fluctuation amplitude is no more than 5%; this is the acceptable range when NPC operates.

In the test scenario, the reference load current in the rating range is determined to be 300 A with a base frequency of 50 Hz. According to the steady state results, the output load current has a standard sinusoidal shape, as shown in Figure 7(a), and no transients exist. A fast Fourier transform (FFT) analysis is performed to check the current quality of the load. The spectral content is calculated up to the 40th harmonic. The total harmonic distortion (THD) value of the load current is shown in Figure 7(b); we see that under steady-state conditions, the total harmonic distortion of the load current is 0.20%, which is a good result. To investigate the instantaneous response of the load current, the process of changing the load value corresponding to the load current is evaluated and shown in Figure 7(c). The results show that the predictive controller quickly responds to the load current. With load variations and error compensation, the voltage value on capacitors does not fluctuate during this period.

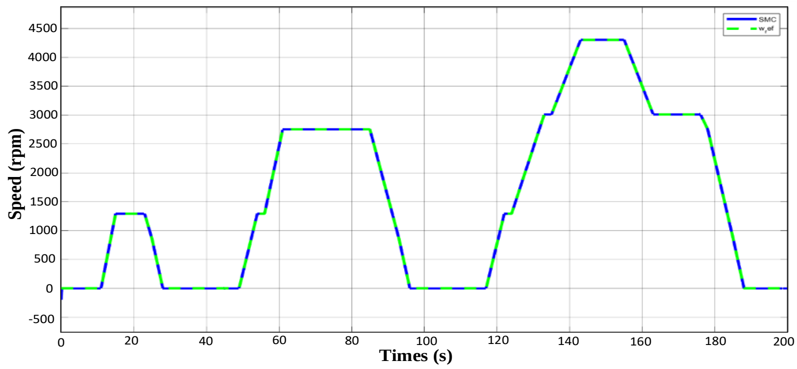

Figure 4. The speed response

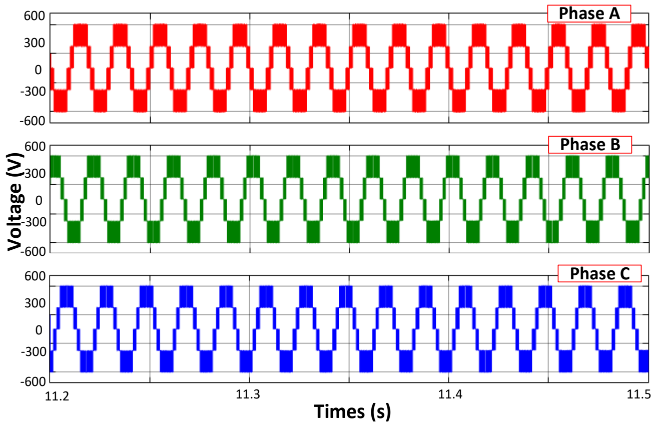

Figure 5. The output voltage value of the NPC inverter

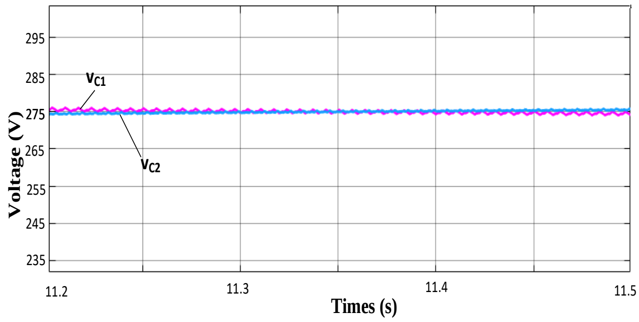

Figure 6. The voltage on capacitors C_1 and C_2 on the DC-link side

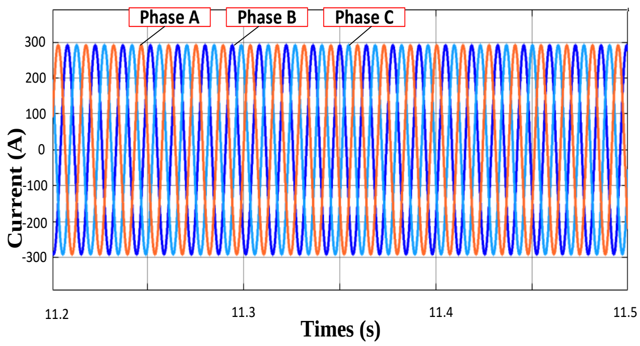

(a)

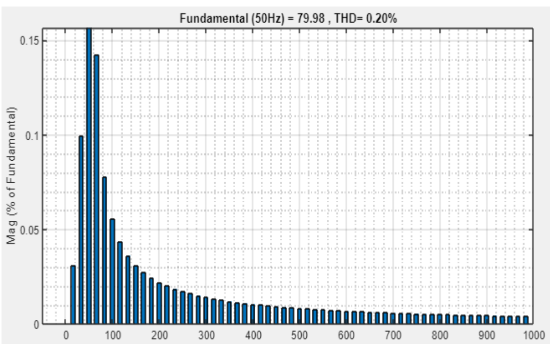

(b)

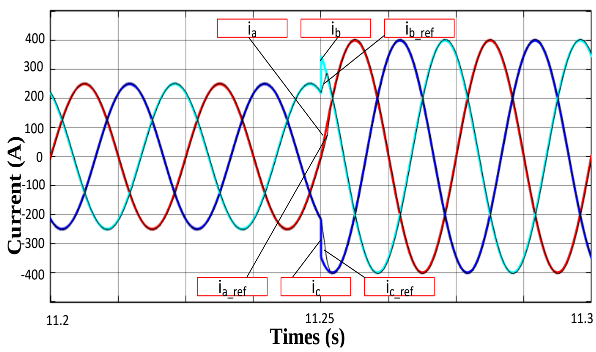

(c)

Figure 7. AC side current result (a) the three-phase current on the load is stable, (b) analyze the THD index of the load current when stable, and (c) the three-phase current on the load varies

5. CONCLUSION

This study proposes an FCS-MPC control strategy with a two-step prediction range to control a three-phase, four-pin NPC converter and applied motor control with an FOC control algorithm. Control process FCS-MPC for two steps has reduced the controller calculation process, reducing the valve switching frequency to an acceptable level. The algorithm result is evaluated by the cost function at the minimum value, corresponding to the value of the load current, has a standard sinusoidal shape with low THD, and the voltage of the DC-Link capacitors is balanced. These values will be predicted for the appropriate switching state to apply to the NPC. The FOC control method is used to control the speed of electric car motors, so they operate well in real situations, increase longevity, protect the engine, and save energy. The proposed method of the article is an excellent solution to control the operation of electric cars. The feasibility of the proposed algorithm was verified by detailed simulation and evaluation.

REFERENCES

[1] J. Becker, C. Schaeper, S. Rothgang, and D. U. Sauer, "Development and validation of an energy management system for an electric vehicle with a split battery storage system," *Journal of Electrical Engineering and Technology*, vol. 8, no. 4, pp. 920–929, Jul. 2013, doi: 10.5370/JEET.2013.8.4.920.

[2] K. Rajashekara, "Present status and future trends in electric vehicle propulsion technologies," *IEEE Journal of Emerging and Selected Topics in Power Electronics*, vol. 1, no. 1, pp. 3–10, Mar. 2013, doi: 10.1109/JESTPE.2013.2259614.

[3] V. F. Pires, D. Foito, and J. F. Silva, "Fault-tolerant multilevel topology based on three-phase H-bridge inverters for open-end winding induction motor drives," *IEEE Transactions on Energy Conversion*, vol. 32, no. 3, pp. 895–902, Sep. 2017, doi: 10.1109/TEC.2017.2693563.

[4] D. Roy, S. Kumar, and M. Singh, "A novel region selection approach of SVPWM for a three-level NPC inverter used in electric vehicle," *International Journal of Power Electronics and Drive Systems*, vol. 10, no. 4, pp. 1705–1713, Dec. 2019, doi: 10.11591/ijpeds.v10.i4.pp1705-1713.

[5] A. Choudhury, P. Pillay, and S. S. Williamson, "Modified DC-bus voltage-balancing algorithm based three-level neutral-point-clamped IPMSM drive for electric vehicle applications," *IEEE Transactions on Industrial Electronics*, vol. 63, no. 2, pp. 761–772, Feb. 2016, doi: 10.1109/TIE.2015.2478392.

[6] X. Jing, J. He, and N. A. O. Demerdash, "Loss balancing SVPWM for active NPC converters," in *2014 IEEE Applied Power Electronics Conference and Exposition - APEC 2014*, Mar. 2014, pp. 281–288, doi: 10.1109/APEC.2014.6803322.

[7] P. Kant and B. Singh, "Multi-pulse AC–DC converter fed SVM controlled NPC inverter based VCIMD," *IET Power Electronics*, vol. 11, no. 14, pp. 2204–2214, Nov. 2018, doi: 10.1049/iet-pel.2018.5084.

[8] H. Vahedi, P. Labbe, and K. Al-Haddad, "Balancing three-level neutral point clamped inverter DC bus using closed-loop space vector modulation: real-time implementation and investigation," *IET Power Electronics*, vol. 9, no. 10, pp. 2076–2084, Aug. 2016, doi: 10.1049/iet-pel.2015.0226.

[9] Y. Li, H. Xiao, N. Jin, and G. Yan, "Model predictive control of NPC three-level grid-tied converter based on reconstructed current," *Archives of Electrical Engineering*, Jan. 2024, doi: 10.24425/aee.2022.140716.

[10] A. Choudhury, P. Pillay, and S. S. Williamson, "Comparative analysis between two-level and three-level DC/AC electric vehicle traction inverters using a novel DC-link voltage balancing algorithm," *IEEE Journal of Emerging and Selected Topics in Power Electronics*, vol. 2, no. 3, pp. 529–540, Sep. 2014, doi: 10.1109/JESTPE.2014.2310140.

[11] U.-M. Choi, J.-S. Lee, and K.-B. Lee, "New modulation strategy to balance the neutral-point voltage for three-level neutral-clamped inverter systems," *IEEE Transactions on Energy Conversion*, vol. 29, no. 1, pp. 91–100, Mar. 2014, doi: 10.1109/TEC.2013.2293502.

[12] S.-J. Chee, S. Ko, H.-S. Kim, and S.-K. Sul, "Common-mode voltage reduction of three level four leg PWM converter," *IEEE Transactions on Industry Applications*, vol. 51, no. 5, pp. 4006–4016, Sep. 2015, doi: 10.1109/TIA.2015.2422771.

[13] Narendra Babu A and P. Agarwal, "Space vector modulation for three-level NPC inverter using two-level space vector diagram," in *2016 IEEE International Conference on Power Electronics, Drives and Energy Systems (PEDES)*, Dec. 2016, pp. 1–6, doi: 10.1109/PEDES.2016.7914563.

[14] U.-M. Choi, F. Blaabjerg, and K.-B. Lee, "Method to minimize the low-frequency neutral-point voltage oscillations with time-offset injection for neutral-point-clamped inverters," *IEEE Transactions on Industry Applications*, vol. 51, no. 2, pp. 1678–1691, Mar. 2015, doi: 10.1109/TIA.2014.2350079.

[15] M. Rivera, V. Yaramasu, A. Llor, J. Rodriguez, B. Wu, and M. Fadel, "Digital predictive current control of a three-phase four-leg inverter," *IEEE Transactions on Industrial Electronics*, vol. 60, no. 11, pp. 4903–4912, Nov. 2013, doi: 10.1109/TIE.2012.2219837.

[16] J. Rodriguez *et al.*, "State of the art of finite control set model predictive control in power electronics," *IEEE Transactions on Industrial Informatics*, vol. 9, no. 2, pp. 1003–1016, May 2013, doi: 10.1109/TII.2012.2221469.

[17] M. Habibullah, D. D.-C. Lu, D. Xiao, and M. F. Rahman, "Finite-state predictive torque control of induction motor supplied from a three-level NPC voltage source inverter," *IEEE Transactions on Power Electronics*, vol. 32, no. 1, pp. 479–489, Jan. 2017, doi: 10.1109/TPEL.2016.2522977.

[18] C. Laoufi, Z. Sadoune, A. Abbou, and M. Akherraz, "New model of electric traction drive based sliding mode controller in field-oriented control of induction motor fed by multilevel inverter," *International Journal of Power Electronics and Drive Systems*, vol. 11, no. 1, pp. 242–250, Mar. 2020, doi: 10.11591/ijpeds.v11.i1.pp242-250.

[19] A. Bendaikha and S. Saad, "Comparative study of five-level and seven-level inverter controlled by space vector pulse width modulation," *International Journal of Power Electronics and Drive System*, vol. 8, no. 2, pp. 755–766, 2017, doi: 10.11591/ijpeds.v8.i2.pp755-766.

[20] A. A. Abdelsalam, M. A. Esmaeel, and S. A. Zaid, "Two-level inverter and three-level neutral point diode clamped inverter for traction applications: a comparative analysis study," *International Journal of Power Electronics and Drive Systems*, vol. 12, no. 3, pp. 1609–1619, Sep. 2021, doi: 10.11591/ijpeds.v12.i3.pp1609-1619.

[21] B. Adda, H. Kada, N. Aouadj, and K. A. Belhia, "New independent control of a Bi Machine system powered by a multi-leg inverter applied to four in-wheel motor drive electric vehicle," *International Journal of Power Electronics and Drive Systems*, vol. 14, no. 1, pp. 614–621, Mar. 2023, doi: 10.11591/ijpeds.v14.i1.pp614-621.

[22] Y. Zhang, W. Cao, S. McLoone, and J. Morrow, "Design and flux-weakening control of an interior permanent magnet synchronous motor for electric vehicles," *IEEE Transactions on Applied Superconductivity*, vol. 26, no. 7, pp. 1–6, Oct. 2016, doi: 10.1109/TASC.2016.2594863.
[23] X. Liu, Z. Q. Zhu, and D. Wu, "Evaluation of efficiency optimized variable flux reluctance machine for EVs/HEVs by comparing with interior PM machine," in *2014 17th International Conference on Electrical Machines and Systems (ICEMS)*, Oct. 2014, pp. 2648–2654, doi: 10.1109/ICEMS.2014.7013948.
[24] J. H. Seo and H. S. Choi, "Cogging torque calculation for IPM having single layer based on magnetic circuit model," *IEEE Transactions on Magnetics*, vol. 50, no. 10, pp. 1–4, Oct. 2014, doi: 10.1109/TMAG.2014.2327204.
[25] B. K. Bose, *Modern power electronics and AC drives*. Prentice Hall, 2022.
[26] T. J. Barlow, S. Latham, I. S. McCrae, and P. G. Boulter, "A reference book of driving cycles for use in the measurement of road vehicle emissions," TRL Published Project Report, 2009.

BIOGRAPHIES OF AUTHORS

Tran Hung Cuong received his engineer (2010); and MSc (2013) degrees in industrial automation engineering from Hanoi University of Science and Technology and completed PhD degree in 2020 from Hanoi University of Science (HUST). Now, he is a lecturer at the Faculty of Electrical and Electronic Engineering at Thuy Loi University (TLU). His current interests include power electronic converters and electric motor drives, converting electricity from renewable energy sources to the grid, and saving energy solutions applied to the grid and transportation. He can be contacted by email: cuongth@tlu.edu.vn.

An Thi Hoai Thu Anh received her engineer (1997) and MSc (2002) degrees in industrial automation engineering from Hanoi University of Science and Technology and completed PhD degree in 2020 from the University of Transport and Communications (UTC). Now, she is a lecturer at the Faculty of Electrical and Electronic Engineering at the University of Transport and Communications (UTC). Her interests include power electronic converter control; electric motor drive control, and energy-saving solutions for industry and transportation. She can be contacted by email: htanh.ktd@utc.edu.vn.